DOI: 10.1002/adma.200702572

Surfactant-Directed Synthesis of Branched Bismuth Telluride/Sulfide Core/Shell Nanorods**

By *Arup Purkayastha, Qingyu Yan, Makala S. Raghuveer, Darshan D. Gandhi, Huafang Li, Zhong W. Liu, Raju V. Ramanujan, Theodorian Borca-Tasciuc,* and *Ganapathiraman Ramanath**

Efficient thermoelectric power conversion and cooling requires materials with high electrical conductivity σ, high Seebeck coefficient α, and low thermal conductivity κ.[1–3] Theory predicts that nanostructuring can increase the figure of merit ZT ($=\sigma\alpha^2T/\kappa$) beyond the bulk value, owing to κ decrease from enhanced phonon scattering at nanostructure boundaries,[4] and increase in σ and α from quantum confinement.[1,5] The promise of higher ZT in nanowires and nanoparticles owing to a greater degree of confinement than in 2D quantum wells[1] has stimulated the exploration of new approaches to synthesize nanostructures of bismuth telluride (Bi_2Te_3-based thermoelectric materials have the highest reported ZT in the bulk form[1,6]) and its alloys.[7–9] Nanorods are of particular interest because they are suitable for building heat-pumping circuits for device cooling, and allow the study of thermal and electrical properties of individual nanostructures through contact formation. Aligned Bi_2Te_3 nanorods can be obtained by electrochemical deposition in porous alumina templates,[10,11] but are typically polycrystalline and exhibit low charge-carrier mobility.[1] Soft-templating approaches utilizing molecular agents are attractive for synthesizing single-crystal nanorods,[12] which are more conducive for high ZT. Moreover, soft-templating can facilitate template removal during processing and harvest template–nanostructure interactions for passivation or doping.[12]

Here, we demonstrate a new approach to obtain core/shell bismuth telluride/bismuth sulfide nanorods with shell branching by using a biomolecular surfactant, L-glutathionic acid (LGTA). We show that crystallographic twinning of Bi_2S_3 driven by Bi-LGTA ligand desorption is the primary mechanism of shell branching, which can be controlled by adjusting the LGTA concentration, reaction temperature, and time. Such branched nanostructures and their formation mechanism are different from the nanotetrapod heterostructures of CdSe and CdTe[13–15] obtained by exploiting lattice mismatch between allotropic polytypes.

In a typical synthesis, we added orthotelluric acid to aqueous $BiCl_3$ in concentrated HNO_3 mixed with LGTA. The solutions were refluxed in a mixture of ethylene glycol and polyethylene glycol (PEG) at 140 or 195 °C for up to 24 hours. Scanning electron microscopy (SEM) images from samples obtained by quenching the reactions at different times reveal nanorods (see Fig. 1) that, upon closer examination, are rectangular prisms with slightly convex facets and lengths ranging between 100–4500 nm. The lateral dimensions span 35–290 nm, and the width of the largest area face of the prism is a factor of 2–3 greater than that of the smaller-face dimension. The nanorod morphology strongly depends on the reaction temperature and time, and LGTA concentration. Reactions with low LGTA/Bi^{3+} ratios at 140 °C for 7 hours $\leq t_{reaction} \leq$ 24 hours yield branched nanostructures (Fig. 1a–c). High LGTA/Bi^{3+} ratios result in unbranched nanorods that are longer and wider (Fig. 1d and e). Increasing the reaction temperature to 195 °C results in longer nanorods, with the reappearance of branches after refluxing for 5 hours (Fig. 1f). Carrying out the reaction at 195 °C for 24 hours yields macroscopic agglomerates, likely resulting from thermally induced degradation of the soft templates. For both LGTA/Bi^{3+} concentration levels, the nanorod length and width increase with increasing reaction time (see Supporting Information Fig. S1), with the latter being smaller.

Metal salt reduction by PEG or LGTA alone does not yield nanorods (see Supporting Information Fig. S2). The former yields micrometer-sized nanoplates with triangular edges, and the latter produces poorly dispersed agglomerates of short (30–150 nm) Bi_2Te_3 nanorods irrespective of reaction time. These results indicate that LGTA is the primary shape-directing agent while PEG serves as a co-surfactant that abets anisotropic growth, probably in a fashion similar to

[*] Prof. G. Ramanath, Dr. A. Purkayastha, Dr. Q. Yan, M. S. Raghuveer, D. D. Gandhi, H. Li
Department of Materials Science and Engineering
Rensselaer Polytechnic Institute
Troy, NY 12180 (USA)
E-mail: ramanath@rpi.edu
Prof. T. Borca-Tasciuc
Department of Mechanical, Aerospace and Nuclear Engineering
Rensselaer Polytechnic Institute
Troy, NY 12180 (USA)
Dr. Z. W. Liu, Prof. R. V. Ramanujan
School of Materials Science and Engineering
Nanyang Technological University
Singapore (Singapore)

[**] We gratefully acknowledge support from the Interconnect Focus Center funded by MARCO, DARPA, and NY state, the National Foundation under grants ECS 0501488 and DMR 0519081, and CTS 0348613, and a research initiation grant from Honda. Supporting Information is available online from Wiley InterScience or from the authors.

ADVANCED MATERIALS

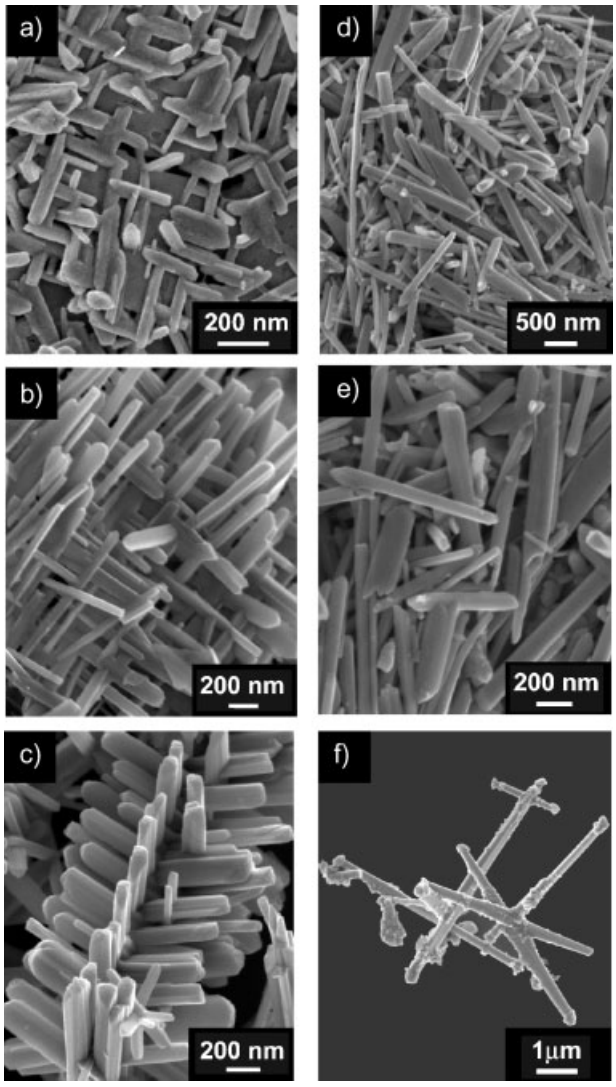

Figure 1. SEM images from nanorods dispersed on a Si(001) substrate with a native oxide. Synthesis at 140 °C with molar ratio LGTA/Bi^{3+} = 10 yields branched nanorods, e.g., for $t_{reaction}$ = 7 h (a), and $t_{reaction}$ = 24 h (b and c). Higher LGTA/Bi^{3+} ratios, e.g., ca. 22, at 140 °C yield unbranched nanorods (d and e). f) A branched nanorod obtained from precursors with LGTA/Bi^{3+} = 22 at 195 °C after 5 h. The H_6TeO_6:PEG ratio was maintained at 0.185:98.4 for all these cases.

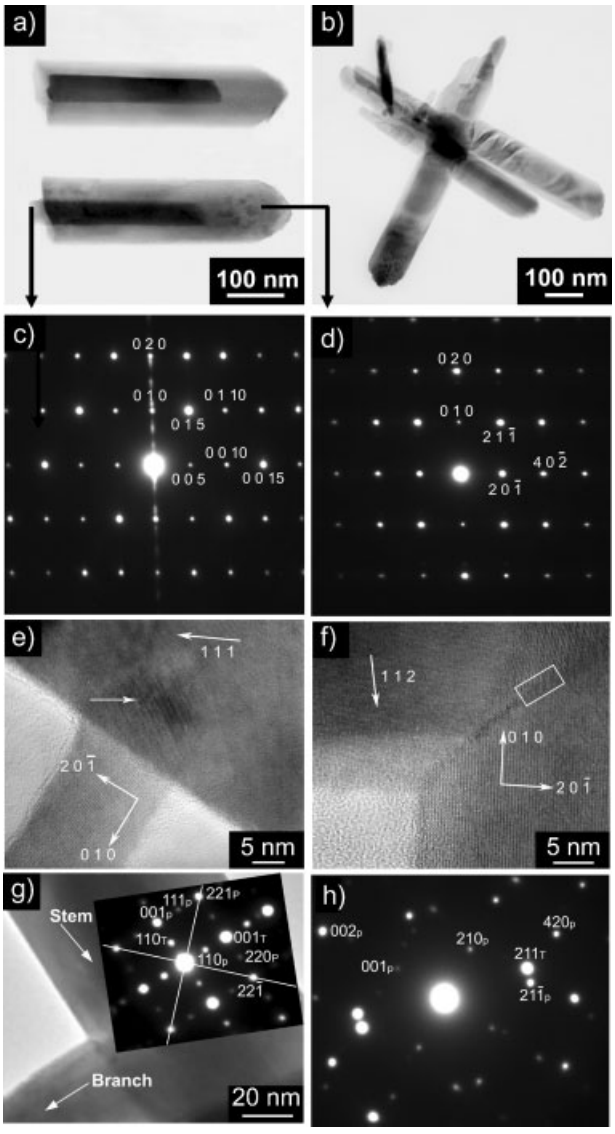

Figure 2. Bright-field TEM images of a) straight and b) branched nanorods. The electron diffraction pattern in (c) is from the Bi_2Te_3or Bi_2Te_2S core (dark contrast, (a)), and that in (d) is from the bismuth sulfide shell (bright contrast in (a)). High-resolution TEM images from stem-branch nodes showing e) Moiré fringes – see arrow – due to overlapping stem and branch shell crystals, and f) an example twin boundary (white box). g) A [1$\bar{1}$0] zone diffraction pattern revealing the twin relationship between the stem and the branch shell, mirrored about the (22 $\bar{1}$) planes of Bi_2S_3. Subscripts ''p'' and ''t'' denote parent and the twinned branch crystals, respectively. h) A [1$\bar{2}$0] zone electron diffraction pattern from another branched structure (not shown).

PEG-assisted growth of Cu and ZnO nanorods.[16,17] Rapid reduction of Bi and Te salts using a strong reductant such as hydrazine monohydrate in the presence of LGTA and PEG also results in macroscopic spheres (see Fig. S2), underscoring the importance of the delicate balance between crystal nucleation and surfactant adsorption–desorption dynamics to obtain anisotropic growth.[18]

Bright-field transmission electron microscopy (TEM) and electron diffraction analyses (see Fig. 2) reveal that the nanorods have a core/shell structure (Fig. 2a) with shell branching (Fig. 2b). The core is either trigonal Bi_2Te_3 or Bi_2Te_2S (see Fig. 2c), and the shell is orthorhombic Bi_2S_3 (Fig. 2d). X-ray diffractograms also show reflections corresponding to these phases (see Supporting Information Fig. S3). The presence of bismuth sulfides suggest that alloying and phase formation occur by decomposition of a thioligated LGTA–Bi^{3+} complex.[19,20] The spot diffraction patterns and uniform contrast in bright field images testify that the core and shell in each nanorod are single crystals with the nanorod axis parallel to [001] of Bi_2Te_3 and [010] of Bi_2S_3. In some cases, we observe hollow shells (e.g., Fig. 2b) suggestive of labile cores

that can slide off the shell. Elongation of the spots along (010) in Figure 2c is likely due to dimensional confinement along this plane normal. High-resolution TEM images from stem-branch nodes of the Bi_2S_3 shell reveal boundaries separating near-orthogonal crystals (Fig. 2e and f) reminiscent of cruciform twinning in orthorhombic minerals.[21,22] This inference is confirmed by electron diffraction patterns from the branching nodes corresponding to twins with a $(22\bar{1})$ mirror plane (see Fig. 2g). Some parent-branch interfaces (see Fig. 2h) reveal a high-angle grain boundary or a twin that does not conform to the usual orthorhombic twin geometries.[21]

X-ray photoelectron spectroscopy (XPS) survey scans from films reveal C, N, O, S, Bi, and Te peaks, while multiplex scans of C 1s and N 1s show amine, amide and carboxyl group signatures from LGTA (see Fig. 3a and b). Spectra from pristine LGTA match well with the spectral signatures seen in the nanorods, except for higher amide/amine sub-band intensity in the latter, suggesting amide formation by reaction between free amines with carboxyl moieties in bismuth sulfide ligated to LGTA during refluxing. Core level S 2s states at 225.3 eV (red band in Fig. 3c) and S 2p at 160.8 eV (blue band in Fig. 3d) confirm the presence of sulfur. The S 2s state is ca. 2.2 eV lower than the free mercaptan signature in pristine LGTA, indicating thio-immobilization on the nanorod surfaces. The Bi 4f band at 158 eV corresponds to $(Bi_2Te_2S)_x(Bi_2S_3)_{1-x}$, consistent with the phases identified by X-ray diffraction (XRD), and is supported by the presence of a Te 3d state at 572.2 eV (see Fig. 3e). The high-binding-energy Bi 4f state near 158.7 eV and the Te 3d state at 575.8 eV indicate the presence of a surface oxide on Bi_2Te_3 nanostructures.[23,24] Because the 15–26 nm thick Bi_2S_3 shell is expected to inhibit oxidation of encapsulated Bi_2Te_3 cores, it is likely that surface oxide forms only on labile core crystals that have slid out of the shell.

Our synthesis approach yields single-crystal core/shell nanorods of Bi_2Te_2S/Bi_2S_3 and Bi_2Te_3/Bi_2S_3 with twinning-induced shell branching in a single synthesis step. Based upon our results, we propose below the phenomenological pathway for the formation, branching, and assembly of core/shell Bi_2Te_3/Bi_2S_3 and Bi_2Te_2S/Bi_2S_3 nanorods. Bi_2Te_3 is formed by PEG reduction of orthotelluric acid and LGTA–Bi^{3+} ion complexes formed via thioligation,[25] consistent with the color change and the core-level band positions of sulfur and bismuth described above. Because LGTA is not known to form micelle-like templates, the underpinning for nanorod growth along ⟨001⟩ is most likely provided by the organization of LGTA–Bi ligands in solution or surfactant-induced growth rate decreases owing to preferential LGTA adsorption on {110},{100}, and {010} crystal facets.[15,16,26] Bi_2S_3 shell formation is driven by the thermal decomposition of thioligated Bi-LGTA complexes on the LGTA-passivated faces of the nanorod surfaces. The presence of Bi_2Te_2S cores suggests simultaneous formation of the core and the shell in some cases. We attribute branching to the opening up of new nucleation

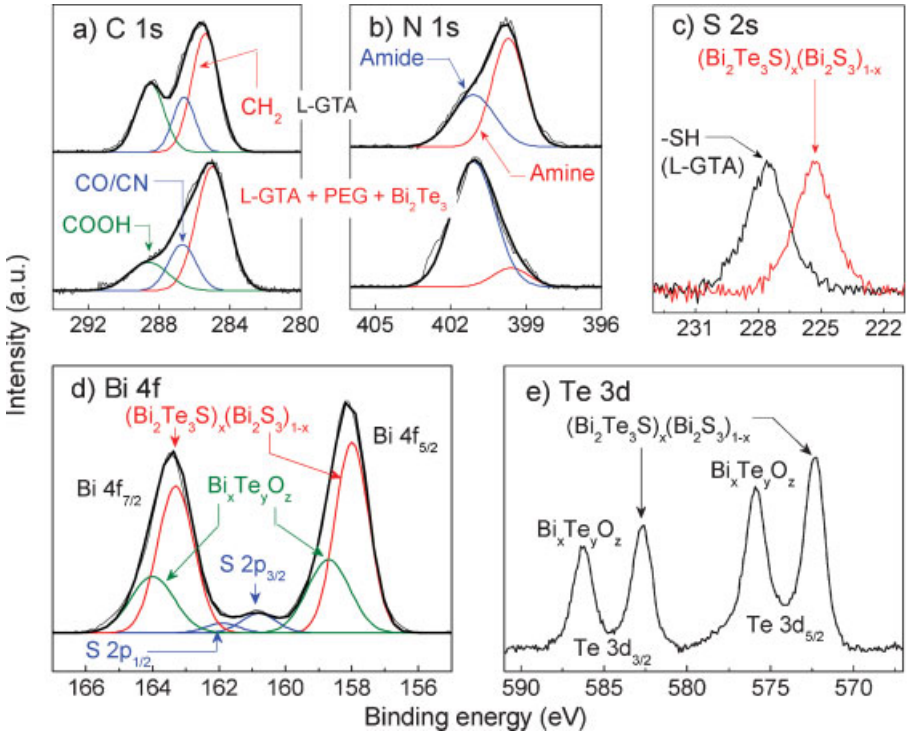

Figure 3. Core-level XPS spectra of LGTA-passivated bismuth telluride nanorods showing a) C 1s, b) N 1s, c) S 2s, d) Bi 4f and S 2p, and e) Te 3d states. Reference spectra from pristine LGTA samples are shown for comparison. The Bi $4f_{7/2}$ and Bi $4f_{5/2}$ sub-bands (red curves) are consistent with the presence of Bi_2S_3, Bi_2Te_2S, and oxidized Bi_2Te_3.

ADVANCED MATERIALS

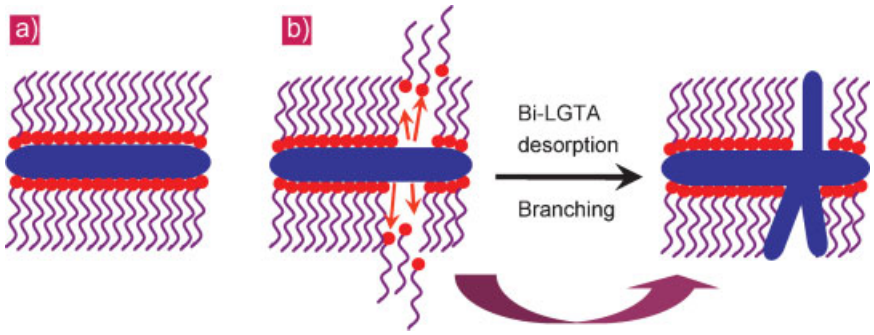

Scheme 1. Illustration of surfactant-induced branching. Straight nanorods grow at high LGTA concentrations (left). Branches are seeded by Bi-LGTA ligand desorption at low LGTA concentrations and high temperature (right).

sites on the nanorod due to increased net desorption of LGTA-Bi complexes either owing to low LGTA concentration or high temperatures. Defects thus created by removal of Bi atoms seed branching through twinning in the Bi_2S_3 shell (see Scheme 1). High LGTA surface coverage of the nanorod surfaces at high concentrations results in low defect density, which suppresses branching. The formation of closely knit nanorod assemblies is attributed to two types of intermolecular bonding between moieties of LGTA on adjacent nanorods, namely, through amide linkages (confirmed by XPS) formed by the coupling of carboxyl and amine moieties, and through hydrogen-bonding between carboxyl and amide groups (see Scheme 2). The lack of surface prefunctionalization to obtain such nanorod assemblies on a native silicon oxide surface renders this approach adaptable to other surfaces, for example, glass, alumina, and possibly biomaterials.

In summary, for the first time we have demonstrated a novel single step approach to synthesize core/shell Bi_2Te_3/Bi_2S_3 and Bi_2Te_2S/Bi_2S_3 nanorods of controllable dimensions in branched and unbranched configurations through the use of a biomolecular surfactant; LGTA. Unbranched nanorods are obtained at high LGTA concentrations and low temperatures. Low LGTA concentrations and high temperatures induce shell branching through crystallographic twinning, owing to defects created by desorption of Bi–LGTA ligands. The presence of carboxyl, amine, and hydroxyl moieties on the nanorod surfaces enables the self-organization and assembly of the nanorods through amidization and hydrogen bonding between functional groups on neighboring nanorods. Such core/shell nanorods and assemblies may offer new possibilities for realization of high-ZT thermoelectric materials and architectures for power generation, nanodevice cooling, nanoscopic thermocouples, smart biomaterials, and biomedical devices.

Experimental

Nanorod Synthesis: All reagents were purchased from Aldrich and were used without further purification. In a typical synthesis bismuth chloride 25.0–33.5 mg (80–107 mmol) was dissolved in 0.4 mL nitric acid. A 0.121–0.162 mmol orthotelluric acid solution was prepared by dissolving 27.7–37.0 mg of the powder in 1 mL water. In another beaker, 323–555 mg (1.07–1.80 mmol) of LGTA was dissolved in 3 mL

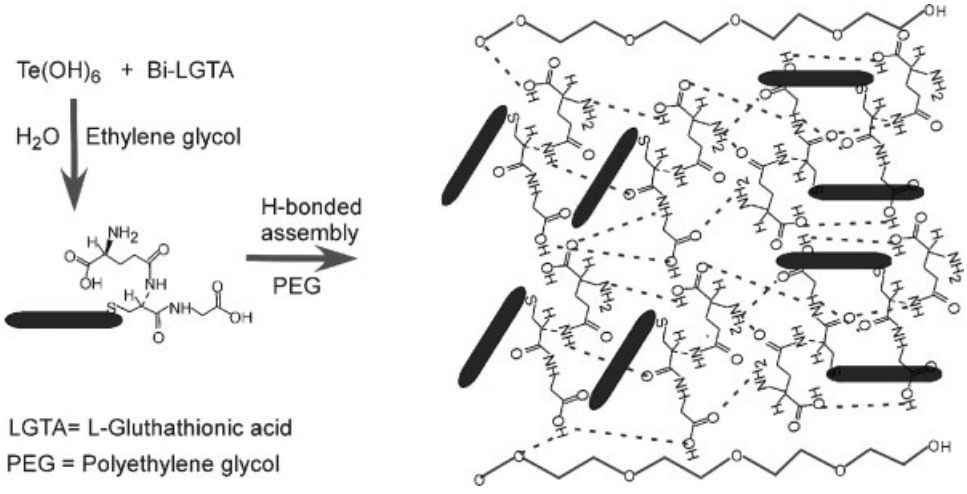

Scheme 2. Illustration of intermolecular hydrogen bonding (denoted by dashed lines) and amidization between the functional groups in LGTA passivating adjacent nanorods, providing the means for nanorod assembly.

water. Slowly adding this LGTA solution to the transparent bismuth chloride solution (*Note*: LGTA reacts violently with bismuth solution, hence the rate of addition is important) transformed the latter into a yellow color because of Bi–LGTA complex formation. The two solutions, that is, those containing Bi and Te, were transferred to a preheated solution of 60 mL ethylene glycol and 4.5–6 mL polyethylene glycol (PEG, $M_n = 600$), and refluxed under vigorous stirring at 140 °C or 195 °C for time intervals up to 24 h. Excess (unligated) surfactants and PEG were removed by repeated centrifuging of the nanostructures first in an ethanol/water mixture, and then in ethanol at 6000 rpm to settle the nanorods at the bottom of the tube, followed by decantation.

Microanalytical Characterization: High-resolution (HR)TEM images and diffraction patterns were obtained using a JEOL 2010 microscope operated at 200 kV. SEM images were obtained using a LEO-SUPRA 55 field-emission instrument operated at 3 kV with a 10 μA beam current. The as-prepared nanorods were dispersed in water, sonicated for 2 min, and drop-cast either over a carbon-coated copper grid for TEM or on a Si(001) wafer piece for SEM and X-ray diffraction, and were air-dried prior to the respective measurements. The X-ray diffractograms were collected using a Scintag diffractometer with a Cu Kα ($\lambda = 0.154$ nm) probe beam. A PHI 5400 instrument with Mg Kα probe beam was used to acquire core-level spectra from nanorod assemblies dispersed on a gold-coated glass substrate.

Received: October 12, 2007
Revised: January 29, 2008
Published online:

[1] G. Chen, M. S. Dresselhaus, G. Dresselhauss, J. P. Fleurial, T. Caillat, *Int. Mater. Rev.* **2003**, *48*, 1.
[2] H. J. Goldsmid, *Thermoelectric Refrigeration*, Plenum, New York **1964**.
[3] G. A. Slack, V. G. Tsoukala, *J. Appl. Phys.* **1994**, *76*, 1665.
[4] M. S. Dresselhaus, G. Dresselhaus, X. Sun, Z. Zhang, S. B. Cronin, T. Koga, J. Y. Ying, G. Chen, *Microscale Thermophys. Eng.* **1999**, *3*, 89.
[5] L. D. Hicks, M. S. Dresselhaus, *Phys. Rev. B* **1993**, *47*, 16631.
[6] L. D. Hicks, M. S. Dresselhaus, *Phys. Rev. B* **1993**, *47*, 12727.
[7] E. J. Menke, Q. Li, R. M. Penner, *Nano Lett.* **2004**, *4*, 2009.
[8] M. Martín-González, A. L. Prieto, R. Gronsky, T. Sands, A. M. Stacy, *Adv. Mater.* **2003**, *15*, 1003.
[9] M. S. Sander, A. L. Prieto, R. Gronsky, T. Sands, A. M. Stacy, *Adv. Mater.* **2002**, *14*, 665.
[10] M. S. Martin-Gonzalez, G. J. Snyder, A. L. Prieto, R. Gronsky, T. Sands, A. M. Stacy, *Nano Lett.* **2003**, *3*, 973.
[11] A. L. Prieto, M. S. Sander, M. S. Martin-Gonzalez, R. Gronsky, T. Sands, A. M. Stacy, *J. Am. Chem. Soc.* **2001**, *123*, 7160.
[12] A. Purkayastha, F. Lupo, S.-Y. Kim, T. Borca-Tasciuc, G. Ramanath, *Adv. Mater.* **2006**, *18*, 496.
[13] D. J. Milliron, S. M. Hughes, Y. Cui, L. Manna, D. J. Li, L.-W. Wang, A. P. Alivisatos, *Nature* **2004**, *430*, 190.
[14] L. Manna, E. C. Scher, A. P. Alivisatos, *J. Am. Chem. Soc.* **2000**, *122*, 12700.
[15] L. Manna, D. J. Milliron, A. Meisel, E. C. Scher, A. P. Alivisatos, *Nat. Mater.* **2003**, *2*, 382.
[16] M. Cao, Y. Wang, C. Guo, Y. Qi, C. Hu. E. Wang, *J. Nanosci. Nanotechnol.* **2004**, *4*, 824.
[17] Z. Li, Y. Xiong, Y. Xie, *Inorg. Chem.* **2003**, *42*, 8105.
[18] J. Chen, T. Herricks, M. Geissler, Y. Xia, *J. Am. Chem. Soc.* **2004**, *126*, 10854.
[19] N. Burford, M. D. Eelman, D. E. Mahony, M. Morash, *Chem. Commun.* **2003**, *146*.
[20] C. O. Monteiro, T. Triodade, *J. Mater. Sci. Lett.* **2000**, *19*, 859.
[21] C. Giacovazzo, *Fundamentals of Crystallography*, Oxford Science, Oxford **1992**.
[22] T. Zoltai, J. Stout, *Mineralogy: Concepts and Principles*, Macmillan, New York **1984**.
[23] H. Bando, K. Koizumi, Y. Oikawa, K. Daikohara, V. A. Kulbachinskii, H. Ozaki, *J. Phys. Condens. Matter* **2000**, *12*, 5607.
[24] A. Purkayastha, S. Kim, D. D. Gandhi, P. G. Ganesan, T. Borca-Tasciuc, G. Ramanath, *Adv. Mater.* **2006**, *18*, 2958.
[25] H. Sun, H. Li, I. Harvey, P. J. Sadler, *J. Biol. Chem.* **1999**, *274*, 29094.
[26] Z. A. Peng, X. Peng, *J. Am. Chem. Soc.* **2001**, *123*, 1389.

